Chemical Science

ROYAL SOCIETY OF CHEMISTRY

EDGE ARTICLE

View Article Online
View Journal | View Issue

Cite this: *Chem. Sci.*, 2022, **13**, 12876

All publication charges for this article have been paid for by the Royal Society of Chemistry

Spatial disposition of square-planar mononuclear nodes in metal–organic frameworks for C_2H_2/CO_2 separation†

Heng Zeng, ‡ Xiao-Jing Xie, ‡ Ying Wang, Dong Luo, Rong-Jia Wei, Weigang Lu * and Dan Li *

Received 3rd August 2022
Accepted 16th October 2022

DOI: 10.1039/d2sc04324f

rsc.li/chemical-science

The efficient separation of acetylene (C_2H_2) from its mixture with carbon dioxide (CO_2) remains a challenging industrial process due to their close molecular sizes/shapes and similar physical properties. Herein, we report a microporous metal–organic framework (JNU-4) with square-planar mononuclear copper(II) centers as nodes and tetrahedral organic linkers as spacers, allowing for two accessible binding sites per metal center for C_2H_2 molecules. Consequently, JNU-4 exhibits excellent C_2H_2 adsorption capacity, particularly at 298 K and 0.5 bar (200 $cm^3\ g^{-1}$). Detailed computational studies confirm that C_2H_2 molecules are indeed predominantly located in close proximity to the square-planar copper centers on both sides. Breakthrough experiments demonstrate that JNU-4 is capable of efficiently separating C_2H_2 from a 50 : 50 C_2H_2/CO_2 mixture over a broad range of flow rates, affording by far the largest C_2H_2 capture capacity (160 $cm^3\ g^{-1}$) and fuel-grade C_2H_2 production (105 $cm^3\ g^{-1}$, ≥98% purity) upon desorption. Simply by maximizing accessible open metal sites on mononuclear metal centers, this work presents a promising strategy to improve the C_2H_2 adsorption capacity and address the challenging C_2H_2/CO_2 separation.

1. Introduction

Acetylene (C_2H_2) is one of the most essential feedstocks in petrochemical industries with a global market of 5.6 billion US$ in 2018 and projected to reach 11.42 billion US$ in 2023.[1] It is manufactured by hydrocarbon cracking or partial nature gas combustion, in which carbon dioxide (CO_2) is an inevitable byproduct.[2] Thus, the removal of CO_2 is a must-do step before further production of value-added chemicals. Yet, the C_2H_2/CO_2 separation is a challenging task owing to their very close molecular sizes/shapes (C_2H_2, 3.34 Å × 3.32 Å × 5.70 Å; CO_2, 3.33 Å × 3.18 Å × 5.36 Å, Fig. S1†) and similar physical properties (boiling points: C_2H_2, 189.3 K; CO_2, 194.7 K).[3] The industrial purification of C_2H_2 from CO_2 is carried out by cryogenic distillation and liquid absorption,[4–7] both of which are highly energy-intensive and often associated with potential safety hazards.

Adsorptive separation enables efficient gas purification and is deemed an energy-saving alternative technology. Porous materials that can selectively adsorb one type of molecule over others have recently aroused great interest and are deemed promising to replace traditional industrial practices. For instance, metal–organic frameworks (MOFs), a.k.a. porous coordination polymers (PCPs), are porous crystalline solids constructed from the self-assembly of organic linkers and metal ions/clusters.[8–20] Although recently emerged, MOFs stand out in gas separation studies and the reticular chemistry enables exquisite control over pore size and surface chemistry to realize preferential binding or even molecular sieving effects.[21–28] With regard to C_2H_2/CO_2 separation, however, the trade-off between adsorption capacity and selectivity still poses a daunting challenge for materials scientists.

Surface engineering with electronegative elements (*e.g.*, N, O, and F) usually facilitates the binding of C_2H_2 over CO_2 due to their difference in the quadrupole moments (-13.4×10^{-40} and $+20.5 \times 10^{-40}$ C m^2 for CO_2 and C_2H_2, respectively) and electrostatic potentials (Fig. S1†).[29–48] For example, a highly fluorinated MOF material SIFSIX-Cu-TPA exhibits a very large C_2H_2 adsorption of 185 $cm^3\ g^{-1}$ at 298 K and 1 bar with a moderate C_2H_2/CO_2 selectivity of 5.4.[31] This approach, however, may not necessarily favor C_2H_2 adsorption as the overall mismatch of electrostatic potentials between the framework surface and C_2H_2 molecule could disrupt and even reverse the selectivity.[49]

College of Chemistry and Materials Science, and Guangdong Provincial Key Laboratory of Functional Supramolecular Coordination Materials and Applications, Jinan University, Guangzhou 510632, P. R. China. E-mail: weiganglu@jnu.edu.cn; danli@jnu.edu.cn

† Electronic supplementary information (ESI) available. CCDC 2160960. For ESI and crystallographic data in CIF or other electronic format see DOI: https://doi.org/10.1039/d2sc04324f

‡ These authors contributed equally.

On the other hand, a more reliable approach is surface engineering with open metal sites (OMSs) to preferentially bind C_2H_2 molecules *via* π-complexation.[50–56] Most of the reported clusters in MOFs offer one accessible OMS per metal, such as mononuclear square-pyramidal,[57] dinuclear paddle-wheel,[58] and trinuclear μ_3-oxo clusters.[59] It is interesting to point out that a simple square-planar mononuclear center may be able to provide as many as two binding sites for C_2H_2 molecules. The material UTSA-74a is constructed with both square-planar and tetrahedral mononuclear zinc centers. Although the square-planar zinc center can provide two accessible binding sites, the tetrahedral one has no accessible binding sites due to the rigid coordination geometry.[51] The material NKMOF-1-Ni is a rare MOF example constructed with square-planar mononuclear centers.[60] As strong as it may seem in the binding of C_2H_2 over CO_2 (C_2H_2/CO_2 selectivity = 249.3), its C_2H_2 adsorption capacity (85.7 $cm^3\ g^{-1}$) is relatively low, likely due to the short Ni···Ni distance (5.75 Å) allowing only one C_2H_2 molecule in between. Intuitively, by employing organic linkers of right size and geometry as spacers, it is plausible to realize the maximum utilization of binding sites of square-planar metal centers, and therefore, achieve not only high C_2H_2/CO_2 selectivity but also large C_2H_2 adsorption capacity (Scheme 1).

Herein we report a microporous MOF (termed JNU-4, JNU = Jinan University) featuring a 4,4-connected **pts** topology with square-planar mononuclear copper(II) centers spaced by tetrahedral organic linkers. Structural analysis shows that every copper center has both OMSs orientated toward the channels, and thus, spatially accessible for C_2H_2 molecules. As a result, the activated JNU-4 (JNU-4a) exhibits excellent C_2H_2 adsorption capacity, particularly at 298 K and 0.5 bar (200 $cm^3\ g^{-1}$). Computational studies confirm that C_2H_2 molecules indeed preferentially occupy both OMSs of the square-planar copper centers, and the simulated adsorption data are consistent with the experimental results. Breakthrough measurements demonstrate that JNU-4a is capable of efficiently separating C_2H_2 from C_2H_2/CO_2 mixtures over a broad range of flow rates, realizing by far the largest C_2H_2 capture capacity and fuel-grade C_2H_2 production even under humid conditions.

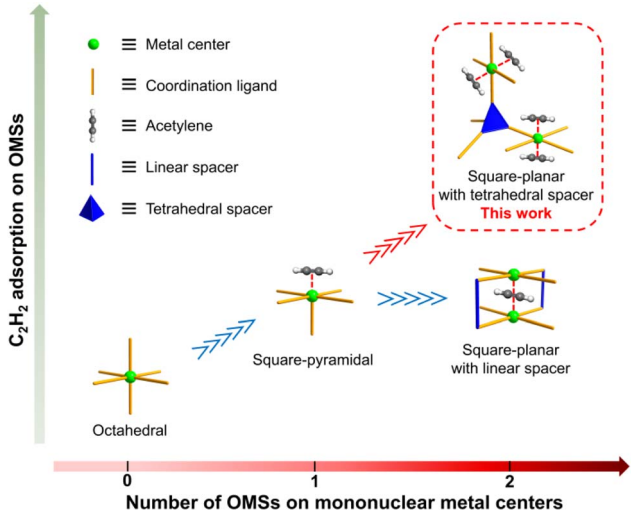

Scheme 1 A simple concept to enhance C_2H_2 adsorption *via* spatial disposition of square-planar mononuclear metal centers with tetrahedral spacers.

2. Results and discussion

2.1. Structure and porosity analysis

JNU-4 was synthesized according to a modified procedure previously reported by Krautscheid.[61] The solvothermal reaction of 5-(3-methyl-5-(pyridin-4-yl)-4*H*-1,2,4-triazol-4-yl)-1,3-benzenedicarboxylic acid (H_2MPTBDC) and $Cu(NO_3)_2\cdot 3H_2O$ in a mixture of acetonitrile, water, and nitric acid yielded dark blue crystals of JNU-4. Single crystal X-ray diffraction (SCXRD) data reveal that the as-synthesized JNU-4 crystallized in the monoclinic $P2_1/c$ space group. There are two crystallographically independent Cu(II) atoms in the asymmetric unit, both of which are in four-coordination with the oxygen/nitrogen atoms of MPTBDC linkers, affording $Cu(COO)_2$(*N*-pyridine)$_2$ and $Cu(COO)_2$(*N*-triazole)$_2$ of similar square planar geometry. One Cu atom coordinates with two O atoms from carboxylate groups and two N atoms from pyridine groups, while the other coordinates with two O atoms from carboxylate groups and two N atoms from triazole groups. The tetrahedral MPTBDC linkers and the square planar copper centers are further linked to generating a three-dimensional (3D) MOF with a 4,4-connected **pts** topology network. The copper centers are sufficiently spaced by the organic linkers and the two binding sites are potentially accessible for C_2H_2 molecules (Fig. 1 and S2†). The phase purity of the bulk JNU-4 was verified by comparison of the simulated and experimental powder X-ray diffraction (PXRD) patterns (Fig. S3†). The N_2 adsorption/desorption measurements of JNU-4a (see the ESI† for the detailed activation method) at 77 K display a reversible type I adsorption isotherm with a saturated adsorption of 400 $cm^3\ g^{-1}$, characteristic of a microporous material (Fig. 2a). The pore size distribution (PSD) calculated using Non-Localized Density Functional Theory (NL-DFT) methods shows two main peaks centered at 4.8 and 9.3 Å (Fig. 2a inset), which are arguably in the right range for realizing

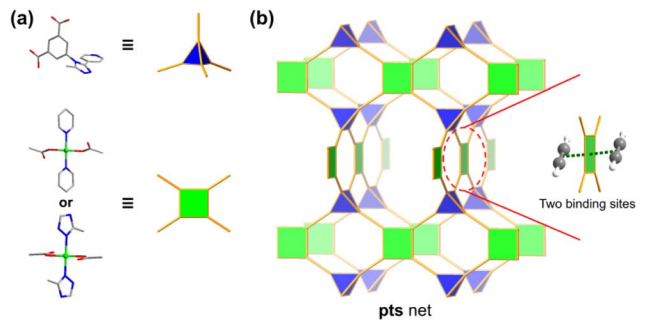

Fig. 1 (a) MPTBDC organic linker as a tetrahedral building unit, $Cu(COO)_2$(*N*-pyridine)$_2$ and $Cu(COO)_2$(*N*-triazole)$_2$ complexes as square-planar 4-connected building units, respectively. (b) Simplified **pts** topology of JNU-4, highlighting that every copper center has both OMSs orientated toward the channels accessible for C_2H_2 interaction. Color code: green, Cu; red, O; blue, N; gray, C. C_2H_2 molecules are shown in a ball-and-stick model depicted in gray.

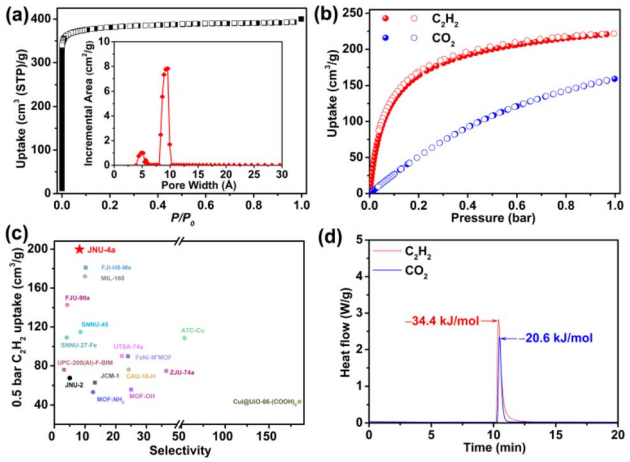

Fig. 2 (a) N_2 adsorption/desorption isotherms of JNU-4a at 77 K. Filled/empty squares represent adsorption/desorption. (Inset) Calculated pore-size distribution using the Non-Localized Density Functional Theory (NL-DFT) method. (b) C_2H_2 and CO_2 single-component adsorption/desorption isotherms of JNU-4a at 298 K up to 1 bar. (c) Comparison of C_2H_2 gravimetric uptake in JNU-4a and some representative MOF materials at room temperature (0.5 bar and 1 bar). (d) Differential scanning calorimetry of JNU-4a upon introducing C_2H_2 or CO_2 at a flow rate of 20 mL min^{-1} under ambient conditions (298 K and 1 bar).

both high C_2H_2 adsorption and C_2H_2/CO_2 selectivity.[62] The Brunauer–Emmett–Teller surface area of JNU-4a was calculated to be 1533 m^2 g^{-1} and the pore volume to be 0.62 cm^3 g^{-1} at P/P_0 = 0.9 (Fig. S4†), which matches well with the crystal structure (0.60 cm^3 g^{-1}), indicating that the sample can be fully desolvated while maintaining the structural integrity. The high surface area, suitable pore size, and square planar mononuclear centers of JNU-4a encouraged us to further investigate its C_2H_2 adsorption and C_2H_2/CO_2 separation. The OMS density of JNU-4a is about 4.8 mmol cm^{-3} (Table S5†), which is mediocre compared to other MOFs, likely due to its high specific surface area (1533 m^2 g^{-1}) and large pore volume (0.62 cm^3 g^{-1}).

2.2. Gas adsorption

Hence, we collected single-component C_2H_2 and CO_2 adsorption isotherms at different temperatures. As expected, JNU-4a manifests a steep adsorption curve with an adsorption capacity of 222 cm^3 g^{-1} at 298 K and 1 bar (Fig. 2b and S5†), which is superior to most of the top-performing materials, such as SIFSIX-Cu-TPA (185 cm^3 g^{-1}),[31] FJU-90a (180 cm^3 g^{-1}),[32] SIFSIX-3-Ni (73.9 cm^3 g^{-1}),[33] ZJU-74a (85.7 cm^3 g^{-1}),[50] UTSA-74a (108 cm^3 g^{-1}),[51] UPC-200(Al)-F-BIM (144.5 cm^3 g^{-1}),[34] FeNi-M′MOF (96 cm^3 g^{-1}),[52] SNNU-27-Fe (182.4 cm^3 g^{-1}),[62] JCM-1 (75 cm^3 g^{-1}),[35] and JNU-1 (64 cm^3 g^{-1}),[63] and slightly lower than that for FJI-H8-Me (229 cm^3 g^{-1}).[64] For an equimolar C_2H_2/CO_2 separation, the C_2H_2 uptake value at a partial pressure of 0.5 bar is considered an essential indicator of its separation potential. JNU-4a exhibits a gravimetric C_2H_2 adsorption capacity of 200 cm^3 g^{-1}. To the best of our knowledge, this value is higher than those of reported top-performance porous materials for C_2H_2/CO_2 separation (Fig. 2c), including MIL-160 (172 cm^3 g^{-1}),[65] Co-MOF-74 (174 cm^3 g^{-1}),[55] SIFSIX-Cu-TPA (168.8 cm^3 g^{-1}),[31] and FJI-H8-Me (180 cm^3 g^{-1}).[64] By contrast, the CO_2 adsorption capacity of JNU-4a at 0.5 bar is 109 cm^3 g^{-1}, which is almost half of that for C_2H_2 under similar conditions. We further employed ideal adsorption solution theory (IAST)[66] to simulate the adsorption behavior for a 50 : 50 C_2H_2/CO_2 gas mixture. As shown in Fig. S6–S8,† JNU-4a shows a moderate IAST selectivity of C_2H_2 over CO_2, reaching up to 8.2 at 298 K and 1 bar, which is higher than that of many benchmark materials studied for C_2H_2/CO_2 separation, such as FJU-90a (4.3),[32] MUF-17 (6.0),[36] SIFSIX-21-Ni (7.8),[38] UPC-200(Al)-F-BIM (3.15),[34] and SNNU-27-Fe (3.6).[62]

2.3. Adsorption enthalpy

To quantitatively depict the large adsorption difference between C_2H_2 and CO_2 on JNU-4a, their isosteric heat of adsorption (Q_{st}) values were calculated from the fitting of single-component gas adsorption isotherms collected at different temperatures. As shown in Fig. S9–S11,† the Q_{st} for C_2H_2 at zero coverage was calculated to be 26.8 kJ mol^{-1}, significantly higher than that for CO_2 (19.7 kJ mol^{-1}). To further experimentally quantify the Q_{st} for C_2H_2 and CO_2 on JNU-4a, we performed differential scanning calorimetry measurements of heat flow upon introducing C_2H_2 or CO_2 at a flow rate of 20 mL min^{-1}, respectively, at 298 K and 1 bar (Fig. 2d). The obtained experimental Q_{st} for C_2H_2 and CO_2 is 34.4 kJ mol^{-1} and 20.6 kJ mol^{-1}, respectively, indicative of a significantly stronger binding affinity for C_2H_2 than CO_2. It is worth mentioning that the Q_{st} for C_2H_2 on JNU-4a is lower than those on UTSA-300 (57.6 kJ mol^{-1}),[67] SIFSIX-3-Ni (36.7 kJ mol^{-1}),[33] and most of the benchmark MOFs with high-density OMSs, such as ATC-Cu (79.1 kJ mol^{-1}),[56] NKMOF-1-Ni (60.3 kJ mol^{-1}),[60] ZJU-74a (45 kJ mol^{-1}),[50] and CuI@UiO-66-$(COOH)_2$ (74.5 kJ mol^{-1})[54] (Fig. S12†). Such a low Q_{st} value implies that JNU-4a could be regenerated under mild conditions, which would be highly beneficial for energy-efficient C_2H_2/CO_2 separation. To prove the easy regeneration and recyclability of JNU-4a, we carried out twenty continuous gas adsorption/desorption measurements for C_2H_2 and CO_2 without applying heat at the degassing stage. As expected, no obvious loss of C_2H_2 and CO_2 adsorption capacity was observed (Fig. S13 and S14†).

2.4. Computational studies

To corroborate the adsorption capacity and the preferred C_2H_2 binding sites in JNU-4a, grand canonical Monte Carlo (GCMC) simulations were first carried out at 298 K.[68,69] The experimental and simulated isotherms are in reasonably good agreement, particularly for C_2H_2 at low pressures and for CO_2 over the entire pressure range (Fig. 3a). The density distribution and radial distribution functions of C_2H_2 and CO_2 at 298 K and 1 bar further reveal that C_2H_2 molecules are indeed predominantly located on both sides of $Cu(COO)_2$(*N*-triazole)$_2$ (site I) and $Cu(COO)_2$(*N*-pyridine)$_2$ (site II), whereas CO_2 molecules were observed only at site I (Fig. 3b, c and S15†). To describe the detailed interactions of gas molecules at both sites, dispersion-corrected density functional theory (DFT-D) calculations were

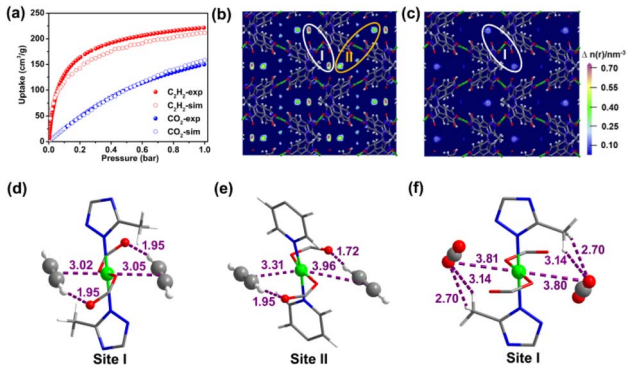

Fig. 3 (a) Experimental and simulated adsorption isotherms of C_2H_2 (red) and CO_2 (blue) at 298 K and up to 1 bar. (b) GCMC simulated adsorption density distributions of C_2H_2 in JNU-4a at 298 K and 1 bar. (c) GCMC simulated adsorption density distributions of CO_2 in JNU-4a at 298 K and 1 bar. (d) DFT-D-calculated binding configurations of C_2H_2 at site I. (e) DFT-D-calculated binding configurations of C_2H_2 at site II. (f) DFT-D-calculated binding configurations of CO_2 at site I (green, Cu; dark gray, C; blue, N; red, O; white, H. C_2H_2 and CO_2 are represented in ball-and-stick models in (d)–(f), and the distance unit is Å).

then carried out. As shown in Fig. 3d–f, two C_2H_2 molecules at site I interact with Cu^{2+} through π-complexation with distances of 3.02 and 3.05 Å, respectively, which are comparable to the sum of the van der Waals radii of carbon (1.70 Å) and copper (1.40 Å) atoms. Additionally, one of the H atoms of C_2H_2 molecules is bound by uncoordinated carboxylate O atoms through C–H···O interaction with a distance of 1.95 Å (Fig. 3d). At site II, two C_2H_2 molecules interact with Cu^{2+} with distances of 3.31 and 3.96 Å, respectively, and both C_2H_2 molecules have an H atom bound by uncoordinated carboxylate O atoms through C–H···O interaction with distances of 1.72 and 1.95 Å (Fig. 3e). By contrast, both CO_2 molecules at site I interact side-on with Cu^{2+} through Cu···O=C=O interaction with distances of 3.80 and 3.81 Å, respectively, and the same interacting O atoms are also bound by H atoms of methyl groups through C=O···H interaction with distances of 2.70 and 3.14 Å, respectively (Fig. 3f). The static binding energies (ΔE) for C_2H_2 were calculated to be 41.7 and 33.2 kJ mol^{-1} at site I and site II, respectively, which is much higher than that for CO_2 at site I (29.87 kJ mol^{-1}). The overall large difference between C_2H_2 and CO_2 in their static binding energies on JNU-4a is in good agreement with their respective experimental Q_{st} values. Thus, not only was the square planar copper center successfully integrated into the framework but also the two OMSs of copper clusters were proved accessible for C_2H_2 binding due to the right-sized organic linker as a spacing unit. The unprecedented maximum utilization of OMSs of the square planar metal center in JNU-4a enables both strong binding of C_2H_2 molecules and large C_2H_2 adsorption capacity, which prompted us to further investigate its C_2H_2/CO_2 separation performance.

2.5. Breakthrough experiments

Column breakthrough experiments were first performed on JNU-4a for a 50 : 50 C_2H_2/CO_2 mixture at a flow rate of 4 mL min^{-1} at 298 K. As shown in Fig. 4a, a clean separation of C_2H_2/CO_2 was observed with a large separation window; CO_2 quickly broke through the column after 42 min g^{-1}, whereas the retention time of C_2H_2 on the column was 79 min g^{-1}, almost doubled that of CO_2. Moreover, the breakthrough curve for CO_2 exhibited a typical but very strong rolling-up at 42 min g^{-1}, with a C/C_0 value rising to 2.0, indicating that a great deal of the adsorbed CO_2 was displaced by C_2H_2 until breakthrough equilibrium, which can be rationalized by their large binding energy difference. Based on the breakthrough curves, the amount of C_2H_2 and CO_2 captured on the breakthrough column was estimated to be 160 cm^3 g^{-1} and 12.5 cm^3 g^{-1}, respectively. Notably, such a captured amount of C_2H_2 is by far the highest among all reported porous materials (Fig. 4b and S17†), including MIL-160 (152 cm^3 g^{-1} or 142 cm^3 g^{-1} in a different report),[65,70] FeNi-M′MOF (66.7 cm^3 g^{-1}),[52] CuI@UiO-66-$(COOH)_2$ (64.7 cm^3 g^{-1}),[54] and ZJU-74 (81.5 cm^3 g^{-1}).[50] With the captured amount of C_2H_2 and CO_2, the separation factor was estimated to be 12.8, which is consistent with the IAST selectivity, and higher than that of most of the top-performing porous materials, such as CuI@UiO-66-$(COOH)_2$ (3.4),[54] FeNi-M′MOF (1.7),[52] FJU-90a (2.1),[32] NKMOF-1-Ni (2.6),[60] and SNNU-45 (2.9)[37] (Fig. S17 and S18†).

Although many MOF materials have been studied for C_2H_2/CO_2 separation, only a few of them reported C_2H_2 purity and

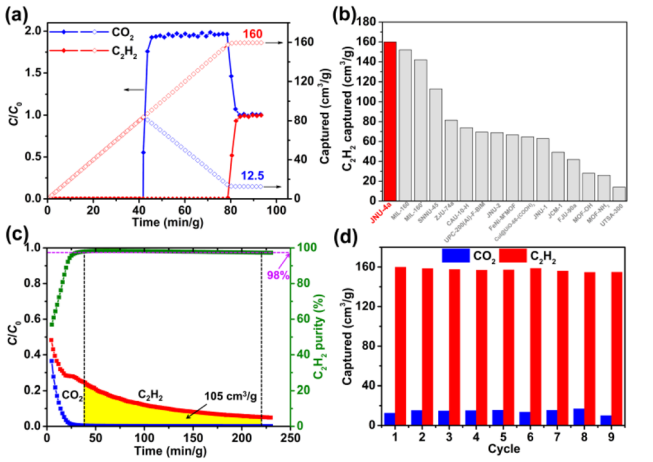

Fig. 4 (a) Breakthrough curves (left y-axis) of C_2H_2 and CO_2 on JNU-4a for an equimolar mixture of C_2H_2/CO_2 (4.0 mL min^{-1}) at 298 K. Empty squares depict the estimated amount of C_2H_2 and CO_2 captured on the breakthrough column (right y-axis). (b) Comparison of the estimated amount of C_2H_2 captured on the breakthrough column for an equimolar mixture of C_2H_2/CO_2 (JNU-4a and other top-performing materials). (c) Desorption curves of C_2H_2 and CO_2 after breakthrough equilibrium with helium gas (10.0 mL min^{-1}) sweeping at 298 K. Solid green squares represent the ratios of C_2H_2/CO_2 in the desorbed gas mixture. The yellow area highlights C_2H_2 with over 98% purity (105 cm^3 g^{-1}) collectible during the desorption. (d) Continuous breakthrough experiments on JNU-4a for an equimolar mixture of C_2H_2/CO_2 at 298 K and the estimated amount of C_2H_2 and CO_2 captured on the breakthrough column of nine cycles. *In situ* regeneration was carried out with helium gas (10.0 mL min^{-1}) sweeping at 298 K.

productivity. The high separation factor of JNU-4a prompted us to conduct desorption experiments. Indeed, fuel-grade C_2H_2 (98% purity) can be achieved upon desorption and the productivity was estimated to be 105 $cm^3\ g^{-1}$ (Fig. 4c and S19†), which is sustainably higher than those of reported porous materials.[33,44,49,71,72] To further evaluate the recyclability of JNU-4a, continuous breakthrough experiments were carried with helium sweeping at room temperature as the regeneration method (Fig. 4d and S20–S22†). Benefitting from its low Q_{st}, JNU-4a maintained the high C_2H_2 capture capacity after nine cycles, highlighting the easy regeneration and good recyclability of JNU-4a for C_2H_2/CO_2 separation. A high diffusion rate is crucial for industrial applications, which will drastically reduce the operation time.[73] Volumetric adsorption kinetics was first studied on a BEL MAX II sorption analyzer; both C_2H_2 and CO_2 exhibit a relatively high diffusion rate with diffusion constants (D/r^2) calculated to be 3.00×10^{-3} and 2.59×10^{-3}, respectively (Fig. S29a and b†). The data were consistent with the time-dependent gravimetric adsorption performed on a thermogravimetric analyzer; both C_2H_2 and CO_2 can reach adsorption saturation in a short time period (Fig. S29c†). To investigate the influence of the flow rate on the separation performance, column breakthrough experiments were carried out for a 50 : 50 C_2H_2/CO_2 mixture at different flow rates (up to 10.0 mL min^{-1}) (Fig. S23–S25†). The breakthrough times of C_2H_2 and CO_2 were reduced with the increase of flow rates, while the amount of the captured C_2H_2 was estimated to be 158.0 $cm^3\ g^{-1}$, 162.4 $cm^3\ g^{-1}$, and 168.3 $cm^3\ g^{-1}$ at flow rates of 6.0 mL min^{-1}, 8.0 mL min^{-1}, and 10.0 mL min^{-1}, respectively. The results suggest that the higher flow rate may increase the amount of C_2H_2 captured on the breakthrough column owing to the buildup of pressures.

In industrial C_2H_2/CO_2 separation, the feed gases may contain water vapor, which will likely affect the separation performance of MOF materials with OMSs. Continuous single-component adsorption/desorption experiments were carried out on JNU-4a with moisturized C_2H_2 (10% relative humidity, RH). As shown in Fig. S26 and S27,† no obvious loss of adsorption capacity was observed after ten cycles of adsorption/desorption. Furthermore, we conducted eight cycles of continuous breakthrough experiments for an equimolar C_2H_2/CO_2 mixture with a flow rate of 6.0 mL min^{-1} under humid conditions (10% RH) (Fig. 5a), and also no obvious loss of capture capacity was observed. The amount of C_2H_2 captured on the breakthrough column was estimated to be 145 $cm^3\ g^{-1}$ (Fig. 5b). Based on desorption curves, about 85 cm^3 of fuel-grade C_2H_2 can be retrieved for 1 g of JNU-4a (Fig. 5c). Although lower than the productivity under dry conditions, it is still much higher than those of reported porous materials, including SIFSIX-3-Ni (56 $cm^3\ g^{-1}$, 99.9%),[33] SIFSIX-dps-Cu (55.6 $cm^3\ g^{-1}$, 99.9%),[71] ZNU-1 (53.8 $cm^3\ g^{-1}$, 99.5%),[44] JXNU-11(Fe_2Ni) (44.3 $cm^3\ g^{-1}$, 95%),[72] and Cd-NP (27.8 $cm^3\ g^{-1}$, 99.99%)[49] (Fig. 5d). Many MOFs with OMSs have been reported to be poisoned by water vapor, and it is worth pointing out that JNU-4a may be capable of efficiently separating C_2H_2/CO_2 even under humid conditions.

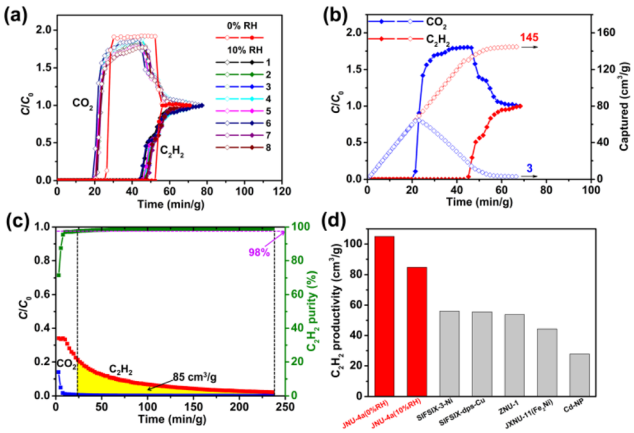

Fig. 5 (a) Continuous breakthrough curves of C_2H_2 and CO_2 on JNU-4a for an equimolar C_2H_2/CO_2 mixture (6.0 mL min^{-1}) under dry (0% RH) and humid conditions (10% RH). *In situ* regeneration was carried out with helium gas (10.0 mL min^{-1}) sweeping at 298 K. (b) One set of breakthrough curves (left *y*-axis) of C_2H_2 and CO_2 on JNU-4a for an equimolar C_2H_2/CO_2 mixture (6.0 mL min^{-1}) under humid conditions (10% RH). Empty squares depict the estimated amount of C_2H_2 and CO_2 captured on the breakthrough column (right *y*-axis). (c) Desorption curves of C_2H_2 and CO_2 after breakthrough equilibrium with helium gas (10.0 mL min^{-1}) sweeping at 298 K. Solid green squares represent the ratios of C_2H_2/CO_2 in the desorbed gas mixture. The yellow area represents C_2H_2 with over 98% purity (85 $cm^3\ g^{-1}$) collectible during the desorption. (d) Comparison of the C_2H_2 productivity estimated from desorption curves for an equimolar C_2H_2/CO_2 mixture.

3. Conclusion

We have implemented a simple concept of two accessible OMSs per metal in MOFs by employing square-planar mononuclear centers as nodes and tetrahedral organic linkers as spacers. The 4,4-connected **pts** topology network (JNU-4) exhibits excellent C_2H_2 adsorption capacity, particularly at 298 K and 0.5 bar (200 $cm^3\ g^{-1}$). Computational modeling studies reveal that C_2H_2 molecules indeed preferentially occupy both OMSs of the square-planar centers. Breakthrough experiments demonstrate by far the largest C_2H_2 capture capacity (160 $cm^3\ g^{-1}$) from a 50 : 50 C_2H_2/CO_2 mixture and fuel-grade C_2H_2 production (105 $cm^3\ g^{-1}$, ≥98%) upon desorption. This work illustrates a straightforward design strategy to maximize the accessible OMSs in MOFs for C_2H_2 adsorption. Further optimization of the spacing linkers with the assistance of computational simulations would be key to advancing in this direction to address the challenging C_2H_2/CO_2 separation.

Data availability

The data that support the plots within this paper and other finding of this study are available from the corresponding authors upon reasonable request.

Author contributions

W. L. and D. L. conceived and designed the research. H. Z., W. L., and D. L. co-wrote the manuscript. H. Z. and X.-J. X. planned

and executed the synthesis, characterization, and gas separation studies. Y. W. performed the theoretical simulations. D. L. and R.-J. W. carried out the structural analyses. All authors participated in and contributed to the preparation of the manuscript.

Conflicts of interest

There are no conflicts to declare.

Acknowledgements

This work was financially supported by the National Natural Science Foundation of China (No. 21731002, 21975104, 21901085, 22271120, 22201101, and 22150004), Guangdong Major Project of Basic and Applied Research (No. 2019B030302009), Guangdong Basic and Applied Basic Research Foundation (No. 2020A1515011005), Innovation Team Project in Guangdong Colleges and Universities (No. 2021KCXTD009), National Postdoctoral Program for Innovative Talent (No. BX20220132 and 2022M711327), and Outstanding Innovative Talents Cultivation Funded Programs for Doctoral Students of Jinan University (No. 2021CXB003).

Notes and references

1 *Acetylene Gas Market Review 2021 and Strategic Plan for 2022 - Insights, Trends, Competition, Growth Opportunities, Market Size, Market Share Data and Analysis Outlook to 2028*, 2022, **https://www.researchandmarkets.com/reports/5460706/acetylene-gas-market-review-2021-and-strategic#tag-pos-1**.
2 A. Granada, S. B. Karra and S. M. Senkan, *Ind. Eng. Chem. Res.*, 1987, **26**, 1901–1905.
3 C. R. Reid and K. M. Thomas, *J. Phys. Chem. B*, 2001, **105**, 10619–10629.
4 S. Chu, Y. Cui and N. Liu, *Nat. Mater.*, 2017, **16**, 16–22.
5 S. Sircar, *Ind. Eng. Chem. Res.*, 2002, **41**, 1389–1392.
6 Q. Qian, P. A. Asinger, M. J. Lee, G. Han, K. MizrahiRodriguez, S. Lin, F. M. Benedetti, A. X. Wu, W. S. Chi and Z. P. Smith, *Chem. Rev.*, 2020, **120**, 8161–8266.
7 D. S. Sholl and R. P. Lively, *Nature*, 2016, **532**, 435–437.
8 H. C. Zhou, J. R. Long and O. M. Yaghi, *Chem. Rev.*, 2012, **112**, 673–674.
9 H. Lyu, O. I.-F. Chen, N. Hanikel, M. I. Hossain, R. W. Flaig, X. Pei, A. Amin, M. D. Doherty, R. K. Impastato, T. G. Glover, D. R. Moore and O. M. Yaghi, *J. Am. Chem. Soc.*, 2022, **144**, 2387–2396.
10 H. Li, L. Li, R.-B. Lin, W. Zhou, Z. Zhang, S. Xiang and B. Chen, *EnergyChem*, 2019, **1**, 100006.
11 N. Hanikel, M. S. Prévot and O. M. Yaghi, *Nat. Nanotechnol.*, 2020, **15**, 348–355.
12 X. Zhao, Y. Wang, D. S. Li, X. Bu and P. Feng, *Adv. Mater.*, 2018, **30**, 1705189.
13 M. Ding, R. W. Flaig, H. L. Jiang and O. M. Yaghi, *Chem. Soc. Rev.*, 2019, **48**, 2783–2828.
14 O. M. Yaghi, M. J. Kalmutzki and C. S. Diercks, *Introduction to reticular chemistry: Metal-organic frameworks and covalent organic frameworks*, Wiley-VCH, Weinheim, 2019.
15 K. Adil, Y. Belmabkhout, R. S. Pillai, A. Cadiau, P. M. Bhatt, A. H. Assen, G. Maurin and M. Eddaoudi, *Chem. Soc. Rev.*, 2017, **46**, 3402–3430.
16 H. Wang, X. Pei, M. J. Kalmutzki, J. Yang and O. M. Yaghi, *Acc. Chem. Res.*, 2022, **55**, 707–721.
17 Z. Ji, T. Li and O. M. Yaghi, *Science*, 2020, **369**, 674–680.
18 H. Wang, Y. Liu and J. Li, *Adv. Mater.*, 2020, **32**, 2002603.
19 Y. Wang, Q. Liu, Q. Zhang, B. Peng and H. Deng, *Angew. Chem., Int. Ed.*, 2021, **130**, 7238–7243.
20 W. Yan, S. Li, T. Yang, Y. Xia, X. Zhang, C. Wang, Z. Yan, F. Deng, Q. Zhou and H. Deng, *J. Am. Chem. Soc.*, 2020, **142**, 16182–16187.
21 B. Chen, S. Xiang and G. Qian, *Acc. Chem. Res.*, 2010, **43**, 1115–1124.
22 J.-R. Li, R. J. Kuppler and H.-C. Zhou, *Chem. Soc. Rev.*, 2009, **38**, 1477–1504.
23 H. Zeng, M. Xie, T. Wang, R.-J. Wei, X.-J. Xie, Y. Zhao, W. Lu and D. Li, *Nature*, 2021, **595**, 542–548.
24 R. B. Lin, Z. Zhang and B. Chen, *Acc. Chem. Res.*, 2021, **54**, 3362–3376.
25 Z.-Q. Zhang, S.-B. Peh, Y.-X. Wang, C.-J. Kang, W.-D. Fan and D. Zhao, *Angew. Chem., Int. Ed.*, 2020, **59**, 18927–18932.
26 R. Matsuda, R. Kitaura, S. Kitagawa, Y. Kubota, R. V. Belosludov, T. C. Kobayashi, H. Sakamoto, T. Chiba, M. Takata, Y. Kawazoe and Y. Mita, *Nature*, 2005, **436**, 238–241.
27 K. J. Chen, D. G. Madden, S. Mukherjee, T. Pham, K. A. Forrest, A. Kumar, B. Space, J. Kong, Q. Y. Zhang and M. J. Zaworotko, *Science*, 2019, **366**, 241–246.
28 C. Gu, N. Hosono, J. J. Zheng, Y. Sato, S. Kusaka, S. Sakaki and S. Kitagawa, *Science*, 2019, **363**, 387–391.
29 C. Graham, J. Pierrus and R. E. Raab, *Mol. Phys. Sci.*, 1989, **67**, 939–955.
30 A. Halkier and S. Coriani, *Chem. Phys. Lett. Sci.*, 1999, **303**, 408–412.
31 H. Li, C. Liu, C. Chen, Z. Di, D. Yuan, J. Pang, W. Wei, M. Wu and M. Hong, *Angew. Chem., Int. Ed.*, 2021, **60**, 7547–7552.
32 Y. Ye, Z. Ma, R.-B. Lin, R. Krishna, W. Zhou, Q. Lin, Z. Zhang, S. Xiang and B. Chen, *J. Am. Chem. Soc.*, 2019, **141**, 4130–4136.
33 K. J. Chen, H. S. Scott, D. G. Madden, T. Pham, A. Kumar, A. Bajpai, M. Lusi, K. A. Forrest, B. Space, J. J. Perry and M. J. Zaworotko, *Chem*, 2016, **1**, 753–765.
34 W. Fan, S. Yuan, W. Wang, L. Feng, X. Liu, X. Zhang, X. Wang, Z. Kang, F. Dai, D. Yuan, D. Sun and H.-C. Zhou, *J. Am. Chem. Soc.*, 2020, **142**, 8728–8737.
35 J. Lee, C.-Y. Chuah, J. Kim, Y. Kim, N. Ko, Y. Seo, K. Kim, T.-H. Bae and E. Lee, *Angew. Chem., Int. Ed.*, 2018, **57**, 7869–7873.
36 O.-T. Qazvini, R. Babarao and S.-G. Telfer, *Chem. Mater.*, 2019, **31**, 4919–4926.
37 Y. P. Li, Y. Wang, Y. Y. Xue, H. P. Li, Q. G. Zhai, S. N. Li, Y. C. Jiang, M. C. Hu and X. Bu, *Angew. Chem., Int. Ed.*, 2019, **58**, 13590–13595.

38 N. Kumar, S. Mukherjee, N. C. Harvey-Reid, A. A. Bezrukov, K. Tan, V. Martins, M. Vandichel, T. Pham, L. M. van Wyk, K. Oyekan, A. Kumar, K. A. Forrest, K. M. Patil, L. J. Barbour, B. Space, Y. Huang, P. E. Kruger and M. J. Zaworotko, *Chem*, 2021, **7**, 3085–3098.
39 S. Dutta, S. Mukherjee, O. Qazvini, A. Gupta, S. Sharma, D. Mahato, R. Babarao and S. Ghosh, *Angew. Chem., Int. Ed.*, 2022, **61**, e202114132.
40 Y. Wang, X. Jia, H. Yang, Y. Wang, X. Chen, A. N. Hong, J. Li, X. Bu and P. Feng, *Angew. Chem., Int. Ed.*, 2020, **59**, 19027–19030.
41 J. Pang, F. Jiang, M. Wu, C. Liu, K. Su, W. Lu, D. Yuan and M. Hong, *Nat. Commun.*, 2015, **6**, 7575.
42 M. L. Foo, R. Matsuda, Y. Hijikata, R. Krishna, H. Sato, S. Horike, A. Hori, J. Duan, Y. Sato, Y. Kubota, M. Takata and S. Kitagawa, *J. Am. Chem. Soc.*, 2016, **138**, 3022–3030.
43 L. Yang, L. Yan, Y. Wang, Z. Liu, J. He, Q. Fu, D. Liu, X. Gu, P. Dai, L. Li and X. Zhao, *Angew. Chem., Int. Ed.*, 2021, **60**, 4570–4574.
44 L. Wang, W. Sun, Y. Zhang, N. Xu, R. Krishna, J. Hu, Y. Jiang, Y. He and H. Xing, *Angew. Chem., Int. Ed.*, 2021, **60**, 22865–22870.
45 Y. Zhang, J. Hu, R. Krishna, L. Wang, L. Yang, X. Cui, S. Duttwyler and H. Xing, *Angew. Chem., Int. Ed.*, 2020, **59**, 17664–17669.
46 W. Gong, H. Cui, Y. Xie, Y. Li, X. Tang, Y. Liu, Y. Cui and B. Chen, *J. Am. Chem. Soc.*, 2021, **143**, 14869–14876.
47 J. Pei, H. M. Wen, X. W. Gu, Q. L. Qian, Y. Yang, Y. Cui, B. Li, B. Chen and G. Qian, *Angew. Chem., Int. Ed.*, 2021, **133**, 2–9.
48 F. Moreau, I. da Silva, N. H. Al Smail, T. L. Easun, M. Savage, H. G. Godfrey, S. F. Parker, P. Manuel, S. Yang and M. Schroder, *Nat. Commun.*, 2017, **8**, 14085.
49 Y. Xie, H. Cui, H. Wu, R.-B. Lin, W. Zhou and B. Chen, *Angew. Chem., Int. Ed.*, 2021, **60**, 9604–9609.
50 J. Pei, K. Shao, J. X. Wang, H. M. Wen, Y. Yang, Y. Cui, R. Krishna, B. Li and G. Qian, *Adv. Mater.*, 2020, **32**, 1908275.
51 F. Luo, C. Yan, L. Dang, R. Krishna, W. Zhou, H. Wu, X. Dong, Y. Han, T.-L. Hu, M. O'Keeffe, L. Wang, M. Luo, R.-B. Lin and B. Chen, *J. Am. Chem. Soc.*, 2016, **138**, 5678–5684.
52 J. Gao, X. Qian, R.-B. Lin, R. Krishna, H. Wu, W. Zhou and B. Chen, *Angew. Chem., Int. Ed.*, 2020, **59**, 4396–4400.
53 S. Liu, X. Han, Y. Chai, G. Wu, W. Li, J. Li, I. da Silva, P. Manuel, Y. Cheng, L. L. Daemen, A. J. Ramirez-Cuesta, W. Shi, N. Guan, S. Yang and L. Li, *Angew. Chem., Int. Ed.*, 2021, **60**, 6526–6532.
54 L. Zhang, K. Jiang, L. Yang, L. Li, E. Hu, L. Yang, K. Shao, H. Xing, Y. Cui, Y. Yang, B. Li, B. Chen and G. Qian, *Angew. Chem., Int. Ed.*, 2021, **60**, 15995–16002.
55 S. Xiang, W. Zhou, Z. Zhang, M. A. Green, Y. Liu and B. Chen, *Angew. Chem., Int. Ed.*, 2010, **49**, 4615–4618.
56 Z. Niu, X. Cui, T. Pham, G. Verma, P. C. Lan, C. Shan, H. Xing, K. A. Forrest, S. Suepaul, B. Space, A. Nafady, A. M. Al-Enizi and S. Ma, *Angew. Chem., Int. Ed.*, 2021, **60**, 5283–5288.
57 E. D. Bloch, W. L. Queen, R. Krishna, J. M. Zadrozny, C. M. Brown and J. R. Long, *Science*, 2012, **335**, 1606–1610.
58 S. S. Y. Chui, S. M. F. Lo, J. P. H. Charmant, A. G. Orpen and I. D. Williams, *Science*, 1999, **283**, 1148–1150.
59 T. Loiseau, L. Lecroq, C. Volkringer, J. Marrot, G. Férey, M. Haouas, F. Taulelle, S. Bourrelly, P. L. Llewellyn and M. Latroche, *J. Am. Chem. Soc.*, 2006, **128**, 10223–10230.
60 Y.-L. Peng, T. Pham, P. Li, T. Wang, Y. Chen, K.-J. Chen, K. A. Forrest, B. Space, P. Cheng, M. J. Zaworotko and Z. Zhang, *Angew. Chem., Int. Ed.*, 2018, **57**, 10971–10975.
61 D. Lässig, J. Lincke, J. Moellmer, C. Reichenbach, A. Moeller, R. Gläser, G. Kalies, K. A. Cychosz, M. Thommes, R. Staudt and H. Krautscheid, *Angew. Chem., Int. Ed.*, 2011, **50**, 10344–10348.
62 Y.-Y. Xue, X.-Y. Bai, J. Zhang, Y. Wang, S.-N. Li, Y.-C. Jiang, M.-C. Hu and Q.-G. Zhai, *Angew. Chem., Int. Ed.*, 2021, **60**, 10122–10128.
63 H. Zeng, M. Xie, Y.-L. Huang, Y. Zhao, X.-J. Xie, J.-P. Bai, M.-Y. Wan, R. Krishna, W. Lu and D. Li, *Angew. Chem., Int. Ed.*, 2019, **58**, 8515–8519.
64 Z. Di, C. Liu, J. Pang, C. Chen, F. Hu, D. Yuan, M. Wu and M. Hong, *Angew. Chem., Int. Ed.*, 2021, **60**, 10828–10832.
65 Y. Ye, S. Xian, H. Cui, K. Tan, L. Gong, B. Liang, T. Pham, H. Pandey, R. Krishna, P. C. Lan, K. A. Forrest, B. Space, T. Thonhauser, J. Li and S. Ma, *J. Am. Chem. Soc.*, 2022, **144**, 1681–1689.
66 A. L. Myers and J. M. Prausnitz, *AIChE J.*, 1965, **11**, 121–127.
67 R. B. Lin, L. Li, H. Wu, H. Arman, B. Li, R. G. Lin, W. Zhou and B. Chen, *J. Am. Chem. Soc.*, 2017, **139**, 8022–8028.
68 D. Dubbeldam, A. Torres-Knoop and K. S. Walton, *Mol. Simul.*, 2013, **39**, 1253–1292.
69 D. Dubbeldam, S. Calero, D. E. Ellis and R. Q. Snurr, *Mol. Simul.*, 2016, **42**, 81–101.
70 Y.-M. Gu, H.-F. Qi, T.-T. Sun, Xi-W. Liu, S. Qadir, T.-J. Sun, D.-F. Li, S.-S. Zhao, D. Fairen-Jimenez and S.-D. Wang, *Chem. Mater.*, 2022, **34**, 2708–2716.
71 J. Wang, Y. Zhang, Y. Su, X. Liu, P. Zhang, R.-B. Lin, S. Chen, Q. Deng, Z. Zeng, S. Deng and B. Chen, *Nat. Commun.*, 2022, **13**, 200–206.
72 X.-P. Fu, Y.-L. Wang, X.-F. Zhang, Z. Zhang, C.-T. He and Q.-Y. Liu, *CCS Chem.*, 2022, **4**, 3416–3425.
73 D. M. Polyukhov, A. S. Poryvaev, A. S. Sukhikh, S. A. Gromilov and M. V. Fedin, *ACS Appl. Mater. Interfaces*, 2021, **13**, 40830–40836.